PNAS RESEARCH ARTICLE | NEUROSCIENCE

Low signaling efficiency from receptor to effector in olfactory transduction: A quantified ligand-triggered GPCR pathway

Rong-Chang Li[a,1], Laurie L. Molday[b], Chih-Chun Lin[a,c,2], Xiaozhi Ren[a,3], Alexander Fleischmann[d], Robert S. Molday[b], and King-Wai Yau[a,1]

Contributed by King-Wai Yau; received November 22, 2021; accepted July 11, 2022; reviewed by Thomas Bozza and Elliott Ross

G protein–coupled receptor (GPCR) signaling is ubiquitous. As an archetype of this signaling motif, rod phototransduction has provided many fundamental, quantitative details, including a dogma that one active GPCR molecule activates a substantial number of downstream G protein/enzyme effector complexes. However, rod phototransduction is light-activated, whereas GPCR pathways are predominantly ligand-activated. Here, we report a detailed study of the ligand-triggered GPCR pathway in mammalian olfactory transduction, finding that an odorant-receptor molecule when (one-time) complexed with its most effective odorants produces on average much less than one downstream effector. Further experiments gave a nominal success probability of tentatively $\sim 10^{-4}$ (more conservatively, $\sim 10^{-2}$ to $\sim 10^{-5}$). This picture is potentially more generally representative of GPCR signaling than is rod phototransduction, constituting a paradigm shift.

GPCR signaling | G protein | signal amplification | olfactory transduction

Significance

G protein–coupled receptor (GPCR) signaling is the most prevalent signaling motif in cells. The basic pathway consists of a GPCR molecule that, once stimulated, goes on to activate a G protein, which in turn typically activates an effector enzyme to produce a cellular function. One long-standing concept about GPCR signaling, originating from a study in rod phototransduction turned into textbook dogma, is high amplification; namely, a large number of downstream G protein molecules are activated by one GPCR molecule. Our findings here from mammalian olfactory transduction now indicate that this amplification is less than unity even for a well-matched odorant/receptor complex. Thus, rod phototransduction is possibly unusual and not necessarily representative of ligand-triggered GPCR signaling generally.

G protein–coupled receptors (GPCRs) are seven–transmembrane domain receptors widely distributed throughout the body and involved in myriad signaling pathways. Although GPCR signaling pathways are predominantly ligand-activated, one particularly well-quantified example is actually rod phototransduction, initiated by light instead of ligand. The occurrence of rod phototransduction in a dedicated, homogeneous cellular compartment (the rod outer segment) has greatly facilitated its quantitative biochemical and biophysical characterizations. Almost 40 y ago, others reported (1) that one photoexcited rhodopsin went on to activate nearly 10^3 downstream transducins (G_{T1}s), hence $G\alpha_{T1}$*/cGMP phosphodiesterase* (PDE*) effector complexes (with "*" meaning active), with a probability of successful transduction literally being roughly $1\text{-}e^{-1,000} = 1.0$. This high biochemical amplification was well-accepted at the time, given that a rod photoreceptor's electrical response to a single photon is large enough to be detectable (2). Over time, this concept of high signal amplification at the G protein step has transcended vision to become a general textbook dogma for GPCR signaling, even though no equivalent suggestion or evidence has emerged in other GPCR pathways, especially those involving ligands. Most recently, we have corrected this long-believed, high amplification in rod phototransduction to be only 10 to 20 (3) (see also ref. 4), albeit still $\gg$1 effector per rhodopsin.

Almost two decades ago, we encountered the same question in vertebrate olfactory transduction (which involves cyclic AMP [cAMP] signaling) in the nasal main olfactory epithelium (5). It is a ligand-triggered GPCR pathway, and has the advantage of occurring also in a dedicated homogeneous compartment (olfactory cilia) of olfactory receptor neurons (ORNs). Olfactory transduction (see refs. 6–8 for reviews) begins when an odorant molecule binds to, and activates, a cognate odorant receptor (OR) (9) on the olfactory cilia (nonmotile in mouse). The odorant/OR* complex activates an olfaction-specific G protein, G_{olf} (10), with its α-subunit ($G\alpha_{olf}$*) in turn activating an olfactory adenylyl cyclase, ACIII (11) (the active effector complex being $G\alpha_{olf}$*/ACIII*), to synthesize cAMP. The resulting elevated cAMP binds to and opens a cyclic nucleotide–gated (CNG) nonselective cation channel (12, 13), causing a membrane depolarization of the cell to firing threshold. A concomitant Ca^{2+} influx through the open CNG channel activates a Ca^{2+}-activated Cl channel (ANO2) (14–17) to lead to a Cl^- efflux, or inward current (18, 19), boosting the depolarizing signal much further (20, 21). This inward Cl current is driven by an atypical steady outward electrochemical gradient for Cl^- maintained by an $Na^+/K^+/Cl^-$ exchanger (22–25). Finally, the cell's recovery from the odorant stimulus involves cAMP hydrolysis by two phosphodiesterases, PDE1C in the cilia (26) and PDE4A in the dendrite and soma (27) (see ref. 8 for updated terminology), as well as Ca^{2+} extrusion (28–32).

In our earlier experiments (5), we happened upon observations that led us to conclude that an OR molecule during its (one-time) binding by, hence complex formation

Author contributions: R.-C.L., R.S.M., and K.-W.Y. designed research; R.-C.L., L.L.M., C.-C.L., and X.R. performed research; A.F. contributed new reagents/analytic tools; R.-C.L. and K.-W.Y. analyzed data; and R.-C.L., R.S.M., and K.-W.Y. wrote the paper.

Reviewers: T.B., Northwestern University; and E.R., University of Texas Southwestern Medical Center.

The authors declare no competing interest.

[1]To whom correspondence may be addressed. Email: rongchangli@gmail.com or kwyau@jhmi.edu.

[2]Present address: Department of Neurology, Columbia University College of Physicians and Surgeons, New York, NY 10032.

[3]Present address: Vedere Bio II, Inc., Cambridge, MA 02139.

This article contains supporting information online at http://www.pnas.org/lookup/suppl/doi:10.1073/pnas.2121225119/-/DCSupplemental.

Published August 1, 2022.

with, an odorant has a very low probability of producing even a single activated $G\alpha_{olf}$*/adenylyl cyclase (ACIII*) effector complex. At the time, the studied ORNs were randomly encountered, each expressing any one of a large number of OR species, and the stimulating odorants were generic ones. As such, the low probability of successful signaling could have simply resulted from a low efficiency of poorly matched odorant/OR complexes. Thus, the crucial question remains: Would a well-matched odorant/OR* complex, as would be the case for most ligand-driven GPCR pathways inside the body functioning with native endogenous ligands, have a high probability of signaling as in rod phototransduction?

To address this question, we have now exploited the timely availability of a unique, genetically engineered M71-monoclonal-nose mouse (33), in which the great majority (>95%) of ORNs in the main olfactory epithelium express predominantly M71-OR, a well-studied OR regarding its odorant preference (34–36). Thus, we have the rare opportunity of focusing on a single OR species in situ. In this study, we have found that the M71-monoclonal-nose mouse ORNs are literal facsimiles of wild-type (WT) M71-expressing ORNs with respect to their levels of olfactory-transduction proteins, including M71-OR. Moreover, the abundance and near homogeneity of the M71-monoclonal-nose ORNs in the main olfactory epithelium allowed us to quantify biochemically the number of M71-OR molecules on one cell, as a potential proxy of ORs generally. By recording electrically from a single isolated ORN from this mouse and stimulating it with precise, quantifiable pulses of acetophenone [among the most effective odorants for M71-OR known so far (34, 35)] such that the number of transient acetophenone/M71-OR* complexes formed during the pulse could be roughly estimated, we succeeded in narrowing down with some level of certainty the probability of a well-matched acetophenone/M71-OR* complex in signaling to the $G\alpha_{olf}$*/ACIII* effector. We found this probability to be very low, nominally on the order of 10^{-4} (more conservatively, $\sim 10^{-2}$ to $\sim 10^{-5}$), or 10,000 times lower than in rod phototransduction. We have also succeeded in quantifying all other proteins in this GPCR signaling pathway.

Altogether, our comprehensive measurements have provided a detailed and quantitative picture of a ligand-triggered GPCR pathway. The overall contrast in signal amplification to rod phototransduction is vast. We think rod phototransduction, owing to its special situation, is quite unusual even compared with cone phototransduction, and olfactory transduction is possibly more indicative of the GPCR signal amplification in general.

Results

Normal Levels of Olfactory-Transduction Proteins Downstream of M71-OR in M71-Monoclonal-Nose ORNs. We generated the M71-monoclonal-nose mouse by crossing the *tet_o-M71-IRES-taulacZ* line (in the *C57BL/6* background) with the *OMP-IRES-tTA* line (in a mixed *129* × *C57BL/6* background) (33), and checked its ORNs for expression of M71-OR against those of WT mice (i.e., WT littermates of the monoclonal-nose mice from the above crossings; Fig. 1*A* and *SI Appendix*, *Text 1*). From real-time RT-PCR, the *M71-OR* messenger RNA (mRNA) level in the bilateral main olfactory epithelium of the monoclonal mice was 1,675 ± 125 times that of WT littermates (mean ± SD, four animals) (Fig. 1*B*), happening to coincide with the $\sim 10^3$ OR molecular species expressed in WT (37, 38).

Next, we checked against WT littermates the monoclonal-nose ORNs' expression of the various olfactory-transduction proteins, namely M71-OR, $G\alpha_{olf}$, ACIII, CNG channel subunits (CNGA2, CNGA4, and CNGB1b), ANO2, PDE1C, and PDE4A, together with OMP [olfactory marker protein (39)] as a reference. The fresh bilateral main olfactory epithelium was completely dissected free from the nasal cavity of a euthanized animal, and the olfactory cilia were detached from the ORN dendrites with an established 20 mM Ca^{2+}/30 mM K^+ shock procedure (40), and then isolated by centrifugation. Subsequent confocal imaging of the deciliated olfactory epithelium immunostained for ACIII and $G\alpha_{olf}$ showed that literally all cilia were detached (*SI Appendix*, Fig. S1*A*). A plant lectin, *Dolichos biflorus* agglutinin, which binds to carbohydrate modifications on a subset of ORs (41), confirmed a largely complete deciliation along with many dendritic knobs, which are distal dendritic swellings from where the cilia emanate (*SI Appendix*, Fig. S1*B*).

Western blotting showed a robust M71-OR band in the M71-monoclonal-nose cilia fraction but not in WT littermates (Fig. 1*C*), due to an expected low percentage (very roughly 0.1% on average) of WT ORNs expressing M71-OR. The antibody against M71-OR (42) actually recognized also M72-OR (*SI Appendix*, *Materials and Methods*), which was, however, likewise invisible in the Western blot as M71-OR for the same reason of low representation. Immunolabeling indicated a strong signal from M71-OR in the cilia layer of unperturbed M71-monoclonal-nose olfactory epithelium, but only weak sporadic signals from M71- and M72-ORs in WT littermates (invisible in Fig. 1*D*; but see *SI Appendix*, Fig. S2). The other olfactory-transduction protein components downstream of M71-OR were also well-segregated according to their known subcellular localizations (Fig. 1 *C* and *D*). Thus, $G\alpha_{olf}$, ACIII, CNGA2, CNGA4, CNGB1b, and ANO2 were all predominantly in the cilia fraction. There was no PDE1C signal in the cilia immunoblot because its antibody worked only in cryosections (Fig. 1*D*), and the converse is true for CNGA4. More importantly, the levels of the transduction proteins downstream of M71-OR were similar across M71-monoclonal-nose animals and WT littermates (Fig. 1*C*). More precise biochemical quantifications are described later (Fig. 8 and *SI Appendix*, Fig. S9).

Taken together, the above suggests that, if M71-OR is expressed in individual M71-monoclonal-nose ORNs also at the same level as in WT M71-expressing ORNs, both sets of ORNs should respond to a given odorant practically identically. This is indeed the case (see below).

Quantitatively Normal Olfactory Responses in M71-Monoclonal-Nose ORNs. We performed suction-pipette recordings in normal Ringer solution at room temperature from ORNs isolated mechanically (*SI Appendix*, *Materials and Methods*) from M71-monoclonal-nose and M71-IRES-tauGFP animals (*SI Appendix*, *Text 1*), with the latter revealing WT M71-expressing ORNs via their selective labeling by green fluorescent protein (GFP). Acetophenone, among the most effective odorants for M71-OR (34, 35), was used for stimulation. At initial screening, a 30-ms, 1 mM acetophenone pulse elicited a saturated response from ~60 to 70% of both M71-monoclonal-nose and M71-IRES-tauGFP ORNs (despite a rare encounter with the latter after dissociation). The nonresponsive ORNs could have 1) lost all of their cilia during mechanical isolation, 2) not survived the dissociation procedure, or 3) (for the M71-monoclonal-nose cells) represented the minor cell population not expressing M71-OR (33). Unfortunately, the cilia of recorded mouse ORNs were just below visibility for evaluation under the optics for electrophysiology. To

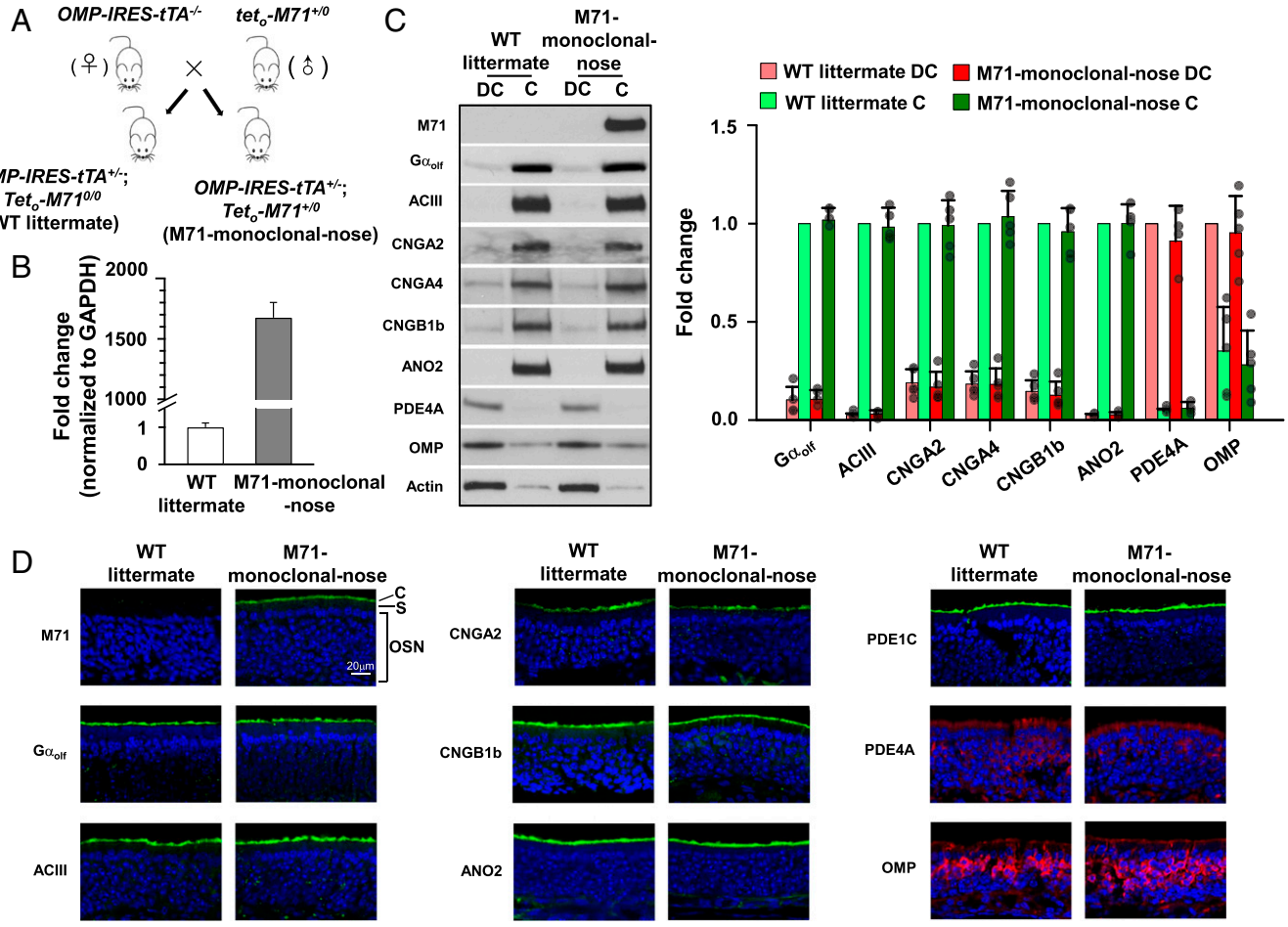

Fig. 1. Normal levels of olfactory-transduction proteins downstream of M71-OR in M71-monoclonal ORNs. (*A*) Schematic diagram showing the genotype of the M71-monoclonal-nose mouse line and its WT littermates. (*B*) Real-time PCR results showing an (~1,675 ± 125)-fold higher *M71-OR* mRNA in M71-monoclonal primary olfactory epithelium compared with that in littermate WT. $n = 4$ animals each. Bars indicate mean ± SD. (*C*, *Left*) Representative Western blot experiments showing the protein expression levels of M71-OR and other transduction components in the olfactory epithelium, which was separated into the cilia fraction (C) and remaining, deciliated epithelium (DC) (*SI Appendix, Materials and Methods*). (*C*, *Right*) The expression levels of the olfactory-transduction components and OMP were comparable between M71-monoclonal-nose mouse and littermate WT. Actin was the loading control. $n = 5$ animals in each group. (*D*) Immunohistochemistry of M71-OR and olfactory-transduction components in cross-sections of main olfactory epithelium from M71-monoclonal-nose mouse and littermate WT mouse. Blue counterstaining was with DAPI to label cell nuclei. C, ciliary layer; OSN, olfactory sensory neuron layer; S, supporting cell layer. (Scale bar, 20 μm.) $n = 3$ animals in each group.

measure dose–response relations, we stimulated a responsive cell with 30-ms acetophenone pulses at 1 μM to 3 mM. Both genotypes showed very similar response sensitivity and kinetics (Fig. 2*A*), especially to weak stimuli (Fig. 2*B*). Within each genotype, the dose–response relation showed an ~10-fold variation in $K_{1/2}$ across cells (Fig. 2 *C* and *D*, *Left*, n_H [Hill coefficient] = 1.15 ± 0.26, $K_{1/2}$ = 135 ± 92 μM [mean ± SD, $n = 13$]; Fig. 2 *C* and *D*, *Right*, n_H = 1.10 ± 0.16, $K_{1/2}$ = 162 ± 149 μM [$n = 8$]), a variation also found by others for M71-IRES-tauGFP ORNs based on Ca^{2+} imaging (34). We interpret this variation in $K_{1/2}$ to reflect likely a variable thin layer of mucus remaining on the cilia to prevent the true bath odorant concentration from reaching the OR (*SI Appendix*, *Text 2* and Fig. S3).

An n_H value close to unity suggests a one-to-one interaction between acetophenone and M71-OR (more in the next section). The saturated response amplitude at high acetophenone concentrations showed a broadly similar range in both genotypes, spanning 33.8 to 311.2 pA for the cohorts of cells in Fig. 2*C* (120.8 ± 47.0 pA for M71-monoclonal-nose ORNs; 146.4 ± 81.8 pA for M71-IRES-tauGFP ORNs). We interpret this amplitude variation to reflect primarily a variable number of lost cilia or partially truncated cilia during mechanical isolation of ORNs. As such, the largest saturated response ever encountered, ~330 pA (see the largest saturated response among the collective data in Fig. 4 *B*, *Right*), should roughly correspond to the saturated response of a fully intact ORN of either genotype. We shall adopt this assumption for later calculations (Fig. 6*B*).

In summary, M71-monoclonal-nose ORNs responded to acetophenone identically as did M71-IRES-tauGFP ORNs, even though an N-terminal Flag-Rho tag exists in the M71 receptor in M71-monoclonal-nose ORNs (33). Thus, the tag had no adverse effect on the function of the M71 receptor. Given the similar sensitivities of the two types of ORNs and their similar levels of downstream transduction proteins as described earlier (see more later), we conclude that M71-monoclonal-nose ORNs also express M71-OR at normal levels. The normal levels of transduction proteins downstream of the OR in monoclonal-nose ORNs are not surprising, owing to their presumably uniform expressions across the main olfactory epithelium. On the other hand, the normal level of M71-OR protein in monoclonal-nose ORNs is not necessarily anticipated, because the mechanism driving M71-OR protein expression in this mouse is not natural (33) (*SI Appendix*, *Text 1*). Thus, most likely, there is a separate mechanism controlling the overall OR protein level in an ORN.

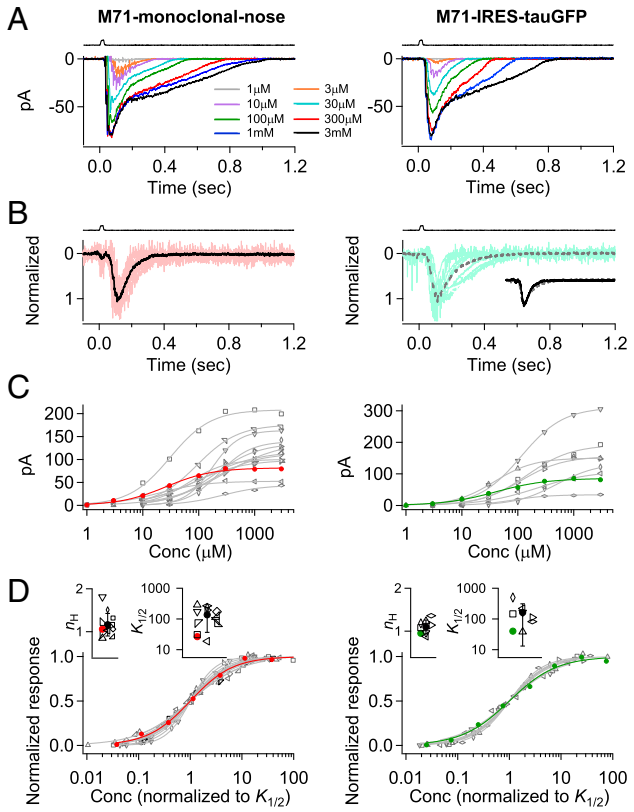

Fig. 2. Normal olfactory signal transduction in M71-monoclonal ORNs. (*Left*) From M71-monoclonal-nose ORNs. (*Right*) From M71-IRES-tauGFP ORNs. (*A*) Odorant response family elicited by 30-ms acetophenone pulses at concentrations of 1 μM to 3 mM. Each family from one cell. Normal Ca^{2+} solution. (*B*) Collective weak responses (<10% of the saturated responses) shown normalized in amplitude to compare their kinetics. Black solid line: cohort average of individual cells (light red); gray dashed line: cohort average of individual cells (light green). (*B*, *Right*, *Inset*) Overlay of solid black and dashed gray responses to indicate essentially identical response kinetics. (*C*) Collective data of dose–response curves from 13 M71-monoclonal-nose cells and 8 M71-IRES-tauGFP cells fitted by the Hill equation. Data indicated in red ($K_{1/2}$ = 26.5 μM, n_H = 1.1) and green ($K_{1/2}$ = 40.0 μM, n_H = 1.0) are from respective response families in *A*. n_H is the Hill coefficient. (*D*) Collective dose–response relations plotted after normalizations by the respective saturated responses and $K_{1/2}$ values. (*D*, *Insets*) n_H and $K_{1/2}$ values from individual ORNs. Red and green data are from the respective cells shown in *C*.

Similar Unitary Electrical Responses of M71-Monoclonal-Nose ORNs and M71-IRES-TauGFP ORNs to Acetophenone or an Even More Effective Odorant. We next examined the unitary electrical response underlying the macroscopic olfactory responses of M71-monoclonal-nose ORNs to acetophenone, by carrying out fluctuation analysis as we had done before (5, 43, 44) on their weak responses. Previously, with such analysis, we have demonstrated that this unitary response in both mouse and amphibian ORNs consists of the electrical effect produced by a single $G\alpha_{olf}$*/ACIII* effector enzyme complex (5, 43, 44). Essentially, the argument is that the probability of an odorant/OR* complex to lead to even just one active downstream $G\alpha_{olf}$*/ACIII* effector is typically so low that the latter becomes the dominant elementary response underlying the trial-to-trial response fluctuations elicited by identical weak odorant pulses (see ref. 3 for an equivalent argument in rod phototransduction). Unlike the previous work (5), which studied randomly encountered ORNs responding to generic odorants, the experiments here examined, importantly, the well-matched acetophenone/M71-OR complex.

To improve the resolution of the unitary response, we used a Ca^{2+}-free external solution (0 Ca^{2+}/1 mM ethylene glycol tetraacetic acid), which removes the Ca^{2+}-mediated negative feedback on transduction (see refs. 7 and 8 for reviews) to increase the amplitude of the weak responses by ∼10-fold, despite concomitantly losing the booster inward Ca^{2+}-activated Cl current (44). Conveniently, removing external Ca^{2+} also largely removed action potentials, making the receptor current much better resolved. To ensure that the responses to weak odorant pulses in Ca^{2+}-free solution summed linearly to allow fluctuation analysis (5), we checked and confirmed a constant response waveform (*SI Appendix*, Fig. S4 *A*, *Inset*) and a linear foot of the dose–response relation typically up to ∼25% of the respective saturated response (*SI Appendix*, Fig. S4 *B* and *C*), which was well beyond the response range that we used for fluctuation analysis. The same linearity was found for M71-IRES-tauGFP ORNs under similar conditions.

Fig. 3 *A*, *Top* shows an experiment on an M71-monoclonal-nose ORN, depicting a subset of the overall stable but widely fluctuating consecutive responses (Fig. 3 *A*, *Bottom*) to 30-ms, 10 μM acetophenone pulses. The overall response-ensemble mean square, $[m(t)]^2$, and variance, $\sigma^2(t)$, had similar waveforms (Fig. 3*B*), suggesting an underlying unitary response with

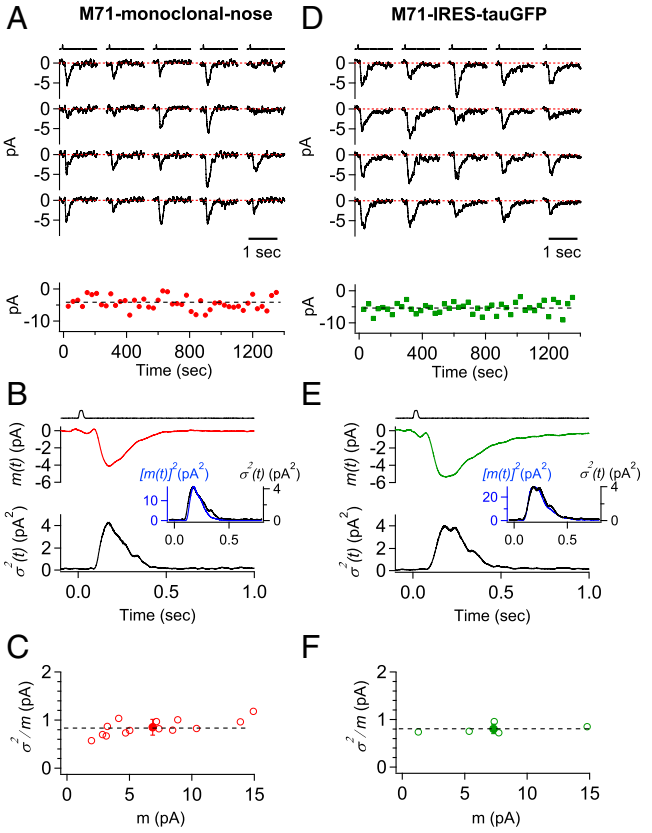

Fig. 3. Unitary electrical response to acetophenone in M71-monoclonal-nose and M71-IRES-tauGFP ORNs. Fluctuation analysis to extract the unitary electrical response in external Ca^{2+}-free Ringer solution at room temperature. Responses elicited by repeated weak, identical odorant pulses (10 μM acetophenone, 30 ms in duration). (*A*–*C*) M71-monoclonal ORNs. (*D*–*F*) M71-IRES-tauGFP ORNs. (*A*, *Upper*) A sample of consecutive responses showing trial-to-trial fluctuations in amplitude (low pass–filtered at 20 Hz). (*A*, *Lower*) Individual response amplitudes (at transient peak) to indicate no progressive change in cell condition over time. Dashed line indicates the level of the mean. (*B*) Response ensemble mean, $m(t)$, and ensemble variance, $\sigma^2(t)$, as a function of time. (*B*, *Inset*) $\sigma^2(t)$ and $[m(t)]^2$ superposed to indicate similar waveforms. (*C*) Collective results of unitary-response amplitude, given by $\sigma^2(t)/m(t)$ at the response's transient peak. Open circles: 14 cells; filled circle: mean ± SD. (*D*–*F*) Similar experiments for M71-IRES-tauGFP–labeled cells. Dashed line indicates the level of the mean. Similar displays for *D*–*F*.

a constant profile. From the Poisson distribution, the unitary-response amplitude is given by the $\sigma^2(t)/m(t)$ ratio, or 1.03 pA at transient peak. This amplitude was quite constant across cells and, as expected, independent of the mean response amplitude, giving 0.85 ± 0.16 pA (n = 14) (Fig. 3*C*). The same experiments on M71-IRES-tauGFP ORNs gave a remarkably similar unitary amplitude of 0.81 ± 0.10 pA (n = 5) (Fig. 3 *D*–*F*), supporting quantitatively similar transduction between M71-monoclonal-nose ORNs and M71-IRES-tauGFP ORNs (*SI Appendix*, *Text 3*).

To verify whether the above unitary response was produced by a single $G\alpha_{olf}$*/ACIII* effector (33), we examined odorants with widely different effectiveness for activating M71-OR (*SI Appendix*, Table S1), and did fluctuation analysis on several of them (Fig. 4). Benzaldehyde and methylsalicylate were less, or much less, effective than acetophenone according to others by Ca^{2+} imaging (35). From the $K_{1/2}$s of their dose–response relations in normal Ca^{2+} solution, we found they were, respectively, ∼(15.5 ± 4.1)-fold (n = 4) and ∼(2,123 ± 1,603)-fold (n = 5) less effective than acetophenone (Fig. 4 *A* and *B*). However, their unitary-response amplitudes and waveforms in Ca^{2+}-free solution were no different from those for acetophenone (benzaldehyde: 0.83 ± 0.22 pA, n = 5; methylsalicylate: 0.83 ± 0.14 pA, n = 5) (Fig. 4 *F* and *G*). In contrast, 2′,4′-dimethylacetophenone, quinoline, and 2′-aminoacetophenone (*Acknowledgments*) were progressively more effective (up to ∼20-fold higher) than acetophenone (Fig. 4 *C*–*E*), but their unitary-response amplitudes and waveforms were again similar (0.69 ± 0.15 pA, n = 3; 0.84 ± 0.20 pA, n = 5; 0.80 ± 0.15 pA, n = 3; respectively) (Fig. 4 *H*–*J*). Thus, a complex between M71-OR and any of these odorants, whether 2,000-fold less effective or 20-fold more effective than acetophenone—an altogether 40,000-fold variation in effectiveness—elicited the same unitary response via a single $G\alpha_{olf}$*/ACIII* effector, implying a very low probability of success (≪1) in triggering transduction across them. Because a probability of ≪1 is still somewhat open-ended, we attempted to narrow the estimate further in the following two sections.

Total Number of M71-OR Molecules on an M71-Expressing ORN. In order to pin down the probability of success further, we needed to correlate the recorded number of electrical unitary responses elicited by an odorant pulse with the estimated number of (one-time) transient acetophenone/M71-OR* complexes

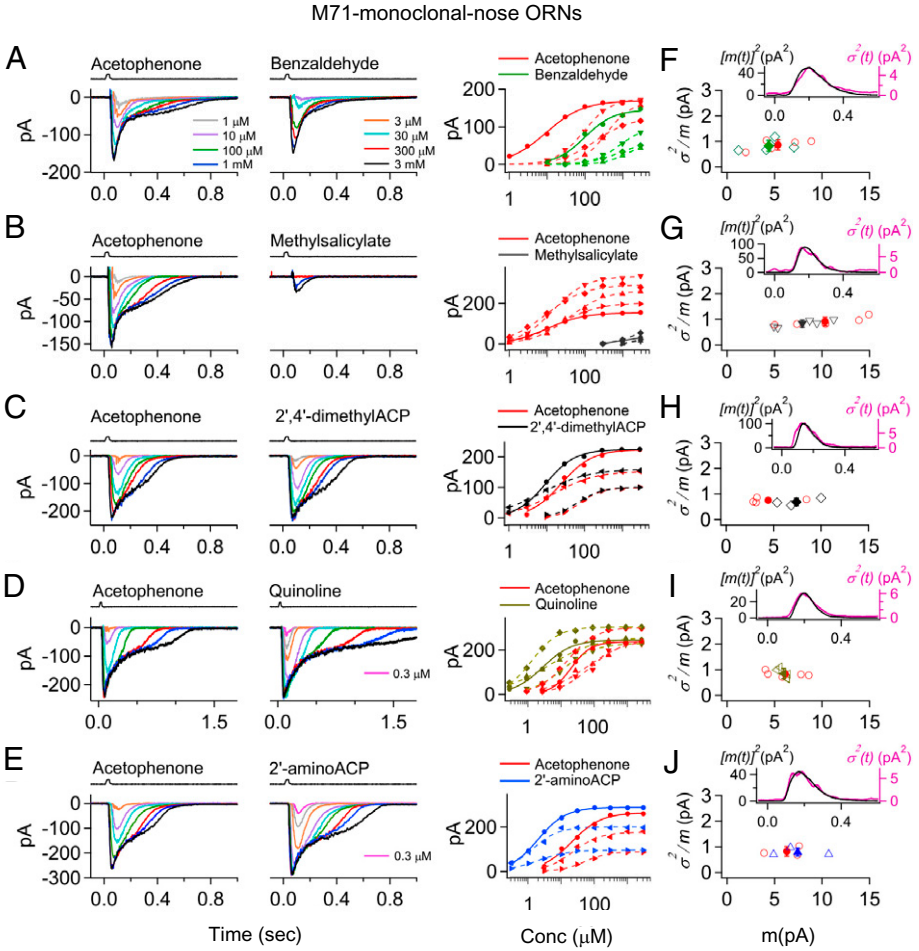

Fig. 4. Similar unitary-response amplitudes of M71-monoclonal ORNs to acetophenone and several odorants with different effectiveness to activate M71-OR. (*A*, *Left*) Odorant response families in normal Ca^{2+} solution, elicited by different strengths (1 μM, 3 μM, 10 μM, 30 μM, 100 μM, 300 μM, 1 mM, and 3 mM, all for 30 ms) of acetophenone (*Left*) and benzaldehyde (*Right*) from the same M71-monoclonal ORN. (*A*, *Right*) Collective data from four cells showing dose–response relations fitted by the Hill equation if complete relations were available, otherwise connected by a straight line. Red solid (acetophenone, $K_{1/2}$ = 9.4 μM, n_H = 0.88) and green solid (benzaldehyde, $K_{1/2}$ ∼100.1 μM, n_H = 1.14) relations are from the cell on the *Left*. Dashed lines are from other cells, with same-shaped symbols in red and green indicating a given cell's respective responses to acetophenone and benzaldehyde. (*B*–*E*) Similar experiments as in *A*, but comparing responses to acetophenone and another odorant: methylsalicylate (*B*), 2′,4′-dimethylacetophenone (*C*), quinoline (*D*), and 2′-aminoacetophenone (*E*). (*F*–*J*) Collective results of unitary responses (measured in zero external Ca^{2+} concentration) elicited by acetophenone, benzaldehyde (*F*), methylsalicylate (*G*), 2′,4′-dimethylacetophenone (*H*), quinoline (*I*), and 2′-aminoacetophenone (*J*). Same format of display as in Fig. 3 *B* and *C*. Signals were low pass–filtered at 20 Hz.

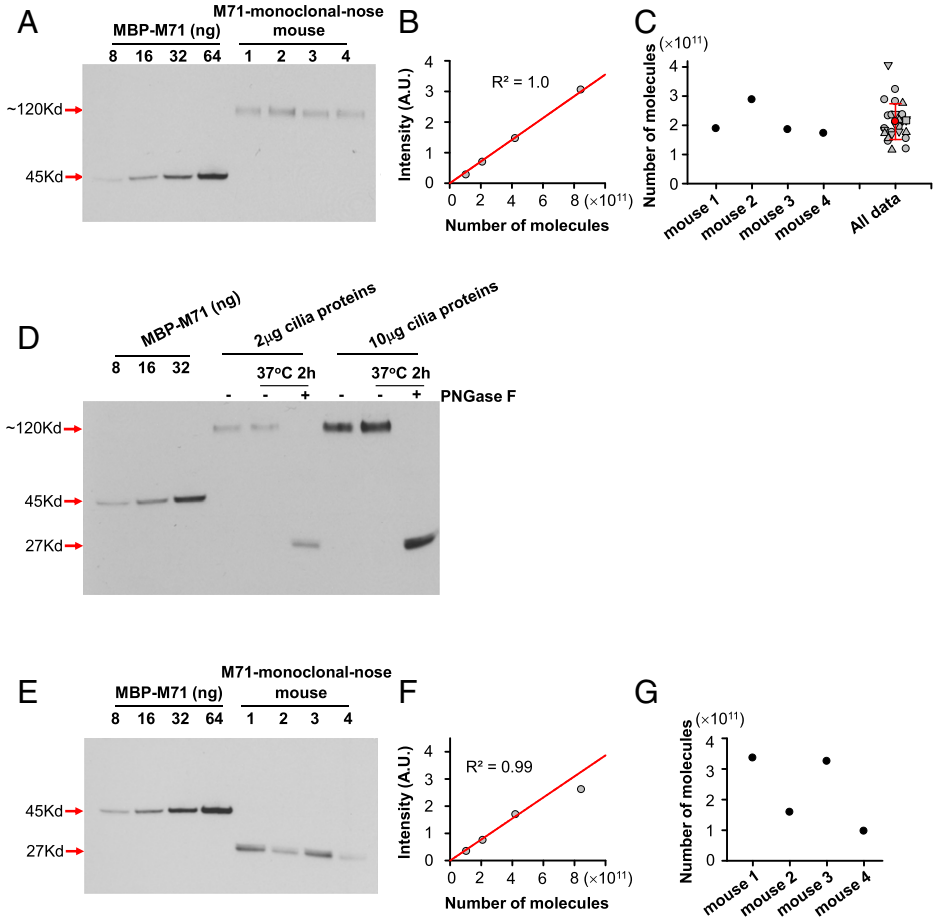

Fig. 5. Quantification of total M71-OR content and its density on olfactory cilia. (*A*) Representative Western blot results showing successive dilutions (8, 16, 32, and 64 ng) of purified MBP-M71 standard proteins (45 kD) (equal to 1.05×10^{11}, 2.10×10^{11}, 4.20×10^{11}, and 8.40×10^{11} molecules), as well as 1/10th of ciliary proteins from each of four separate M71-monoclonal mice in the same blot. (*B*) The signal intensities of different amounts of MBP proteins were plotted against molecule numbers (gray dots). The standard curve (red) was fitted linearly. $R^2 = 1.0$, indicating the signal intensity of the band was fully proportional to the number of molecules of MBP. A.U., arbitrary unit. (*C*) Number of M71-OR molecules in 1/10th of ciliary proteins from each of four separate M71-monoclonal mice (black dots) and the average (red dot) from 29 mice (gray). (*D*) Ciliary proteins (2 and 10 μg) were treated with or without PNGase F at 37 °C for 2 h. Incubation of cilia fraction at 37 °C without PNGase F for 2 h serves as a control to demonstrate that incubation at 37 °C without PNGase F for 2 h will not degrade the M71-OR. (*E*) Purified MBP standard proteins (8, 16, 32, and 64 ng), as well as 1/10th of PNGase F–treated ciliary proteins from each of four mice, were loaded onto the same gel. (*F*) A standard curve was obtained by plotting the signal intensity against the number of molecules. (*G*) Numbers of M71-OR molecules in 1/10th PNGase F–treated ciliary proteins from each of four mice.

formed during the pulse. To estimate the latter parameter, we had to measure with biochemistry the total number of M71-OR molecules on an M71-monoclonal-nose ORN.

We started by expressing a tagged M71-OR protein heterologously in HEK293 cells (*SI Appendix, Materials and Methods*). After purifying the recombinant protein with the tag, we found that it migrated on a gel at the expected molecular mass of the monomer (~27 kDa), but also as dimeric and higher-order complexes (*SI Appendix*, Fig. S5), as seen for rhodopsin (45), which affect quantification. We next switched to the pMAL protein fusion and purification system, by inserting the complementary DNA coding for M71-OR's C terminus (which contains the epitope sequence for our M71-OR antibody) into a pMAL vector downstream of the *malE* gene coding for the maltose-binding protein (MBP). As shown in Fig. 5*A*, the purified fusion protein after expression in *Escherichia coli* was recognized by our M71-OR antibody to give a specific signal. With successive dilutions, we generated a standard curve relating protein-band intensity and different amounts of the purified MBP-M71-OR fusion protein for calibrations (Fig. 5*B*). To quantify the number of M71-OR molecules in the cilia fraction of the bilateral olfactory epithelium, we loaded 1/10th of the cilia fraction from each of four M71-monoclonal-nose mice into different lanes of a gel together with the standard fusion protein (Fig. 5*A*). From the standard curve, the number of M71-OR molecules in each loaded cilia fraction (1/10th of total) could be obtained (Fig. 5*C*), giving 1.89, 2.88, 1.85, and 1.73×10^{11} molecules, respectively. A repeat experiment from another four M71-monoclonal-nose mice is shown in *SI Appendix*, Fig. S6. Altogether, from 29 animals, the average number of M71-OR molecules in 1/10th of the ciliary fraction per mouse was $(2.13 \pm 0.61) \times 10^{11}$ (Fig. 5 *C*, *Far Right*). Thus, there are overall $\sim 2 \times 10^{12}$ M71-OR molecules in an M71-monoclonal-nose mouse's bilateral main olfactory epithelium, or $\sim 2 \times 10^{5}$ M71-OR molecules per ORN, given that there are $\sim 10^{7}$ ORNs in the mouse tissue (46–48).

According to its position in the gel, the apparent size of M71-OR from the cilia fraction was about ~120 kDa (Fig. 5*A*), close to four times that of the monomeric molecular mass (~27 kDa). Even as a dimer, which at least many GPCRs are known to form, the molecular mass should not be at 120 kDa. Possibly, M71-OR in the native olfactory epithelium is heavily glycosylated. Accordingly, we treated the ciliary proteins with the deglycosylating enzyme, PNGase F, for 2 h at 37 °C. After treatment, the purified M71-OR protein band indeed shifted to ~27 kDa (Fig. 5*D*), similar to the recombinant M71-OR

monomer expressed in HEK293 cells (*SI Appendix*, Fig. S5). Exposure to 37 °C for 2 h without PNGase F did not affect the band position of M71-OR, nor did PNGase F treatment significantly change its amount (Fig. 5*D*). A quantification of the deglycosylated protein as described above with MBP-M71-OR fusion protein as a standard gave (2.29 ± 1.20) × 10^{12} M71-OR molecules (four animals) per bilateral olfactory epithelium (Fig. 5 *E*–*G*), comparable to that in non–PNGase F–treated proteins.

The total number of OR molecules per ORN is all that is necessary for further calculations. However, it is convenient to know the density of M71-ORs on the cilia membrane. Apart from being an indicator of its degree of packing, it is a useful parameter for biophysical calculations. Based on the cilium diameter measured with electron microscopy, as well as the number and the length of cilia measured with immunohistochemistry in conjunction with confocal microscopy, we obtained a total ciliary surface area of ∼140 μm^2 for M71-monoclonal-nose ORNs (*SI Appendix*, *Text 4* and Fig. S7), and a similar ciliary surface area for M71-IRES-tauGFP ORNs (*SI Appendix*, Fig. S7 *B* and *D*). Longer cilia lengths, however, were reported by others with somewhat different labeling methods capable of revealing the slender apical parts of the cilia (49, 50) (*SI Appendix*, *Text 4*), giving an up to 50% larger total calculated ciliary surface area of 210 μm^2. We adopted this latter value as being more accurate for subsequent calculations, bearing in mind, however, that calculations involving only the overall molecular populations on an ORN are not affected.

Dividing the above ∼2 × 10^5 M71-OR molecules per ORN by 210 μm^2, we get ∼1,000 OR molecules per square micrometer on the cilia, assuming a uniform cilia OR density over the ciliary surface.

Narrowing Down the Probability of an Acetophenone/M71-OR* Complex in Producing Downstream $G\alpha_{olf}$*/ACIII* and Hence Transduction. To narrow down the probability of an acetophenone/M71-OR* complex in producing a $G\alpha_{olf}$*/ACIII* effector, we measured the strength of an odorant pulse (odorant concentration × duration) required for eliciting on average one elementary (unitary) electrical response. The precise temporal configuration of the solution change around the recorded ORN could be assessed from the junction current created by switching from normal Ringer to 90% Ringer (5). Although not exactly identical in shape to the rectangular electronic command pulse, the time-integrated odorant pulse area was nonetheless very similar (*SI Appendix*, Fig. S8*A*; also see *SI Appendix*, *Text 5* and Fig. S8*B*). Based on the physics of diffusion, this time-integrated odorant stimulus can be converted into a rough number of transient collisions between odorant molecules and a given M71-OR molecule. This number is then multiplied by the total M71-OR population on the recorded cell's cilia (see below) to give the total number of collisions between the odorant and OR on the entire cell during the odorant pulse. This number on a mechanically isolated ORN is expected to vary from experiment to experiment due to partial damage (see an earlier section) and, ideally, should be estimated just before the cell is recorded. However, with fluorescence imaging of the GFP labeling in M71-IRES-tauGFP ORNs under the optics for electrophysiology, we were only able to detect the cilia at their bases but not in their entirety even with overexposure of the fluorescence (Fig. 6*A*). As an alternative, we used the saturated response of a recorded cell as an indicator of its degree of intactness, by assuming the largest saturated response ever encountered from M71-monoclonal-nose ORNs or M71-IRES-tauGFP ORNs (330 pA; see earlier text associated with Fig. 2 *C* and *D*) to correspond to the fully intact situation in terms of cilia number and length as described in the previous section, and proportionally lower ciliary membrane surface areas (hence fewer OR molecules) for cells with lower saturated responses (see Fig. 6*B* for the ORNs described in this section). In this way, we could evaluate the total number of M71-OR molecules on a particular isolated ORN under recording, assuming a uniform distribution of M71-ORs and its downstream olfactory-transduction components on the ciliary surfaces.

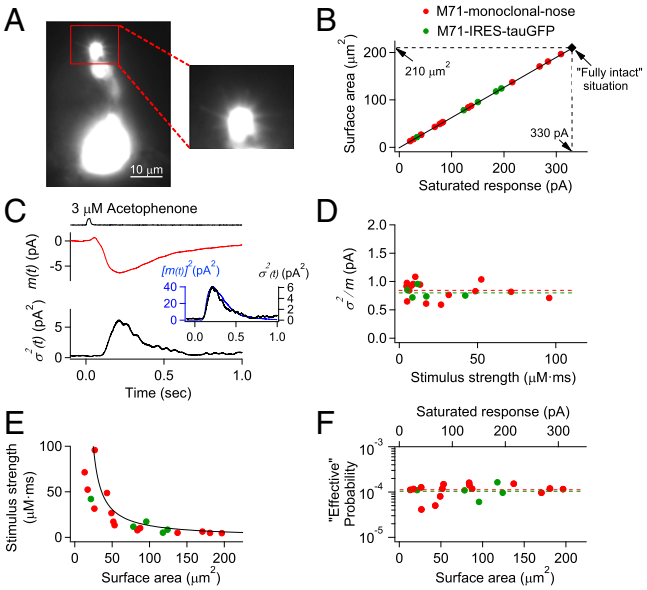

Fig. 6. Order-of-magnitude estimate of the probability of one acetophenone/M71-OR complex* successfully producing a downstream $G\alpha_{olf}$*/ACIII* effector complex. (*A*) Representative image of a mechanically dissociated ORN from an M71-IRES-tauGFP mouse immediately before suction-pipette recording. The GFP signal was overexposed in order to visualize the cilia inside the red rectangle. Only the basal end of a cilium can be visualized; 100× objective. (*B*) Relation for calculating the surface area of an ORN's cilia based on the cell's saturated response, by assuming that the largest encountered saturated response (330 pA) corresponds to the intact overall ciliary surface area (210 μm^2). Lower saturated responses would have proportionally lower membrane surface areas. Altogether, 15 M71-monoclonal ORNs (red) and 5 M71-IRES-tauGFP ORNs (green) are associated with the experiment presented in this figure. (*C*) Response ensemble mean, $m(t)$ (red trace), and ensemble variance, $\sigma^2(t)$ (black trace), from one M71-monoclonal ORN elicited by a repeated 3 μM, 30-ms pulse of acetophenone in zero external Ca^{2+} concentration. (*C*, *Inset*) $\sigma^2(t)$ and $[m(t)]^2$ superposed to indicate similar waveforms. Signals were low pass–filtered at 20 Hz. (*D*) Collective results of unitary-response amplitude calculated from $\sigma^2(t)/m(t)$ at the response's transient peak, and independent of stimulus strength. Fifteen M71-monoclonal ORNs (red; dashed line indicates average) and five M71-IRES-tauGFP ORNs (green; dashed line indicates average). (*E*) Stimulus strength required for producing one successful elementary (unitary) electrical response is inversely proportional to a given cell's ciliary surface area (smooth curve). Red: 15 cells from M71-monoclonal ORNs; green: 5 cells from M71-IRES-tauGFP ORNs. (*F*) Probability of one acetophenone/M71-OR complex to produce one $G\alpha_{olf}$*/ACIII* effector complex is quite constant across different ORNs with different ciliary surface areas. Red: M71-monoclonal ORNs; green: M71-IRES-tauGFP ORNs. Dashed lines are averages. Room temperature.

By fluctuation analysis of a series of weak responses in the linear range elicited by repeated identical acetophenone pulses in Ca^{2+}-free Ringer at room temperature as described before, we extracted the unitary-response amplitude as well as its multiplicity of occurrence in a pulse trial (equivalent to the "quantal content" in presynaptic vesicular release), with the latter being given by the ratio $[m(t)]^2/\sigma^2(t)$ at the transient peak of the response. Thus, in the linear response range, the acetophenone pulse strength required for eliciting exactly one unitary response could be calculated based on proportionality. Fig. 6*C* shows

one such experiment, giving a unitary amplitude of 0.95 pA and a multiplicity of 6.7 events for a 30-ms, 3 μM pulse of acetophenone.

For free diffusion of a small molecule such as acetophenone in aqueous solution, its collision rate with a fixed target at room temperature is in the range of $\sim 10^8$ to $\sim 10^{10}$ $M^{-1}{\cdot}s^{-1}$ with a nominal "consequential" rate (i.e., those collisions that successfully lead to odorant/OR complex formation) of perhaps 10^8 $M^{-1}{\cdot}s^{-1}$ (51). This lower rate reflects steric effects such that only a fraction of the collisions would lead to complex formation. For a 30-ms, 3 μM pulse of acetophenone, this gives $\sim 10^8$ $M^{-1}{\cdot}s^{-1} \times (3 \times 10^{-6}$ M$) \times (30 \times 10^{-3}$ s$) = 9$ consequential collision events per OR molecule during the pulse. Multiplying this number by the total ciliary M71-OR population on this particular cell, namely 1,000 $\mu m^{-2} \times 53.1$ μm^2 (with the latter value being the ciliary surface area read from Fig. 6*B* based on this cell's saturated response of 83.5 pA), we obtained an overall 4.78×10^5 acetophenone/OR complex-formation events on the cell. Dividing this number by the measured 6.7 unitary electrical effects, we arrived at 7.13×10^4 acetophenone/OR complex-formation events required for eliciting one unitary response, that is, a probability of success of 1.40×10^{-5}. Correcting for the apparent mucus barrier that we have detected (Fig. 2), we increased this success probability by up to 10-fold, giving 1.40×10^{-4}.

Collective data from 15 M71-monoclonal-nose ORNs gave a unitary response of 0.84 ± 0.15 pA (Fig. 6*D*). The strength of the acetophenone pulse required for eliciting this response ranged from 4.6 to 95.7 μM·ms (i.e., pulse concentration × pulse duration), and was inversely proportional to the respective cell's ciliary surface area (Fig. 6*E*, red circles), as derived from its saturated response amplitude (Fig. 6*B*). This observed inverse proportionality supports our rationale of using a cell's saturated response to extract its ciliary area, as well as the notion that the components of olfactory transduction, including M71-OR, are generally uniformly distributed along the cilia and that olfactory transduction constitutes spatially localized events surrounding the active OR molecules (5, 43, 44, 52). From collective data, the mean probability of an acetophenone/M71-OR* complex to activate one $G\alpha_{olf}$*/ACIII* was nominally $(1.08 \pm 0.33) \times 10^{-4}$ (Fig. 6*F*, red circles). In summary, the probability of success is indeed very low. We have also carried out the same experiments on M71-IRES-tauGFP ORNs, giving results agreeing well with those from M71-monoclonal-nose ORNs (Fig. 6 *E* and *F*, green symbols).

The above narrowed-down nominal probability of success is based on the assumption that the commonly adopted consequential on-rate of $\sim 10^8$ $M^{-1}{\cdot}s^{-1}$ (51) applies, ignoring elaborate geometrical considerations of OR molecules situated on cylindrical cilia (53, 54). In the absence of actual measurements, a broader, more conservative range for the consequential on-rate—10^6 to 10^9 $M^{-1}{\cdot}s^{-1}$—may be more appropriate, borrowed from a host of enzyme–substrate interactions (see table 7.3 in ref. 51 and table 4.3 in ref. 55), giving a success probability of $\sim 10^{-2}$ to $\sim 10^{-5}$. Even the high-end probability arrived at here of $\sim 10^{-2}$ is nonetheless still very low, and quantitatively consistent with our simple and direct conclusion from the experiments in Fig. 4 that the probability is $\ll 1$ even for well-matched odorant–OR complexes.

In search of the weak link in the olfactory-transduction cascade underlying the above low probability of success, we attempted to measure the dwell time of acetophenone on M71-OR after complex formation by examining the dependence of the response amplitude on the duration of an acetophenone pulse at response-saturating concentrations (0.3 to 1 mM) (see ref. 5 for strategy). Previously, with this strategy and using randomly encountered WT ORNs and generic odorants, we found a dwell time that was below our experimental resolution—perhaps 1 ms or less (5). Unfortunately, acetophenone is so effective in eliciting a response that even a pulse as brief as 20 ms at such concentrations elicited a response beyond the linear range, with shorter pulse durations not feasible, owing to the finite speed of our solution-switching device for applying and removing odorant (*SI Appendix, Materials and Methods*).

We next tried to analyze the kinetics of the linear response (i.e., to a weak odorant pulse) for assessing this parameter in the presence of external Ca^{2+}. Because the normal olfactory response is composed of the cAMP current closely followed by the inward Cl current, we removed the Cl current in normal Ca^{2+} solution by using the *Ano2*$^{-/-}$ genetic background so as to isolate the cAMP pathway (21). The notion behind this approach is that the slowest step in a signaling cascade is typically indicated by the final decay of the linear impulse response, regardless of the order of its occurrence in the cascade (see, for example, ref. 56). Fig. 7, *Left*, shows the weak responses of an *Ano2*$^{-/-}$ M71-monoclonal-nose ORN to a 30-ms pulse of, respectively, 3 μM acetophenone, 0.3 μM 2′-aminoacetophenone (20-fold more effective than acetophenone), and 300 μM methylsalicylate (2,000-fold less effective than acetophenone). The kinetics of the responses to all three odorants are remarkably similar. In particular, their final decays are all describable by a single-exponential, with a time constant ($\tau_{recovery}$ or τ_{rec}) of 53.7, 56.3, and 62.2 ms, respectively (Fig. 7, *Left*, dashed curves). Collective data for τ_{rec} from altogether seven cells gave a mean ± SD of 48.2 ± 10.4 ms (acetophenone), 50.2 ± 7.4 ms (2′-aminoacetophenone), and 53.5 ± 15.8 ms (methylsalicylate). The very similar τ_{rec}s across these odorants of vastly different efficiencies suggest that τ_{rec} is probably not the odorant dwell time on M71-OR; otherwise, one would expect a strong correlation between efficiency and dwell time, especially given that we have previously found no evidence

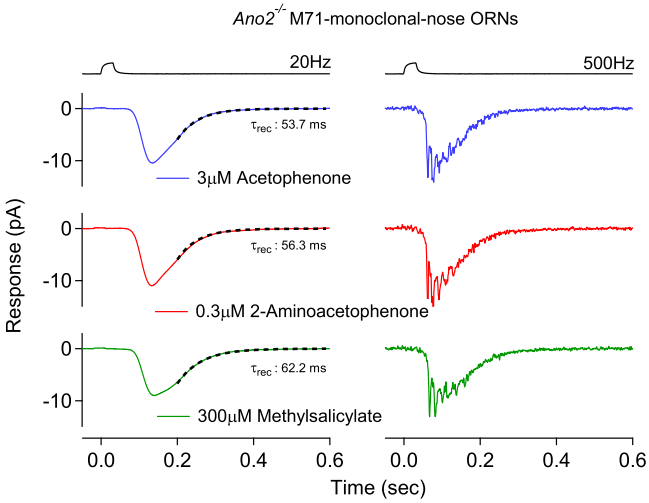

Fig. 7. Longest recovery time constant of a weak response triggered by three different odorants with widely different efficacies in activating an M71-OR. Representative weak responses triggered by 30-ms pulses of 3 μM acetophenone (blue; *Top*), 0.3 μM 2′-aminoacetophenone (red; *Middle*), and 300 μM methylsalicylate (green; *Bottom*) in the same ORN from the *Ano2*$^{-/-}$; M71-monoclonal-nose mice. Normal external Ca^{2+} concentration. Each response was averaged from ≥30 traces. (*Left*) Signals were low pass–filtered at 20 Hz. (*Right*) Signals were low pass–filtered at 500 Hz. The recovery phase of a weak response was fitted by a single-exponential decline function (black dashed line), showing the similar time constants (τ_{rec}) among different odorants with different effectiveness to activate M71-OR.

of fast inactivation of the ligand/receptor complex by receptor phosphorylation at least for weak odorant pulses (5) (see also ref. 57). Thus, the odorant dwell time is probably shorter than τ_{rec}. Extracting it, if possible at all, requires knowing more about the precise rising shape of the response and its precise temporal delay with respect to the odorant pulse, which unfortunately were confounded by action potentials (Fig. 7, *Right*) distorting the response's rising kinetics, and by mucus on the cilia delaying the response slightly. Attempts to eliminate the Na and Ca action potentials with tetrodotoxin and other blockers in the presence of external Ca^{2+} were hampered by some effects on the response shape. Removing external Ca^{2+} greatly reduced the presence of action potentials (see earlier section), but this condition is unphysiological by removing negative feedback via Ca^{2+} on transduction.

What is the interpretation of τ_{rec} ~50 ms? It likely reflects a downstream signaling step. One possibility is the lifetime of $G\alpha_{olf}$*, which in turn dictates the lifetime of ACIII*. τ_{rec} is too slow to reflect the gating of CNG channels, which happens within a few milliseconds and with no intrinsic desensitization (58). Interestingly, the corresponding τ_{rec} in rods' dim-flash response (~200 ms at 37 °C) also corresponds to $G\alpha_{T1}$*'s lifetime (56). Most recently, the lifetimes of heterologously expressed $G\alpha_{olf}$* and its closest relative, $G\alpha_s$*, have been measured to be much longer, being on the order of seconds (59) (see also ref. 60 for $G\alpha_s$*) in the absence of the associated GAP (GTPase accelerating protein) or RGS (regulator of G protein signaling) protein yet to be identified (if they exist at all) for accelerating their deactivation (59, 61). If our interpretation of τ_{rec} is correct, how $G\alpha_{olf}$*'s lifetime is shortened so much in situ remains unknown.

Mole Ratios of Key Protein Components in Olfactory Transduction. Our Western blot data presented earlier (Fig. 1*C*) have demonstrated roughly normal levels of the olfactory-transduction components downstream of M71-OR in the M71-monoclonal-nose mouse. With our success in quantifying biochemically the total number of M71-OR molecules on an ORN's cilia from this mouse, we decided to do the same for these proteins.

Standard protein samples of $G\alpha_{olf}$, ACIII, CNGA2, and ANO2 were generated as described above by using the pMAL fusion protein and purification system, consisting of fusing our antibody-directed epitope sequences in the above proteins to the C terminus of MBP followed by expression and purification (*SI Appendix, Materials and Methods*). Fig. 8 *A*, *Left* shows the various fusion proteins: MBP-$G\alpha_{olf}$, MBP-ACIII, MBP-CNGA2, and MBP-ANO2, together with MBP-M71 (as reference), recognized by their respective antibodies, along with their standard calibration curves relating band-signal intensity to the number of MBP fusion-protein molecules based on dilutions (Fig. 8 *A*, *Middle*). Each set of data for the proteins shown in Fig. 8*A* was obtained from the same M71-monoclonal-nose mouse (designated 1, 2, 3, etc.) or WT littermate. Altogether, 21 M71-monoclonal-nose and 13 WT littermate mice were used (with the former being a subset of monoclonal-nose animals distinct from those shown in Fig. 5*A* and *SI Appendix*, Fig. S6; see the legend for Fig. 8*A*). All collective data are shown in Fig. 8 *A*, *Right* (with solid black symbols indicating the data from the three M71-monoclonal-nose animals and the three WT littermates in Fig. 8 *A*, *Left*). As in Fig. 5*A* and *SI Appendix*, Fig. S6, the number of molecules indicated in each case represents only 1/10th of the cilia fraction. As such, the respective total absolute protein molecular amounts in the cilia of M71-monoclonal ORNs are $(2.09 \pm 0.50) \times 10^{12}$ for M71-OR, $(29.72 \pm 8.32) \times 10^{12}$ for $G\alpha_{olf}$, $(1.14 \pm 0.33) \times 10^{12}$ for ACIII, $(0.46 \pm 0.18) \times 10^{12}$ for CNGA2, and $(1.44 \pm 0.53) \times 10^{12}$ for ANO2, giving mole ratios of 100 M71-OR: 1,422 $G\alpha_{olf}$: 54.5 ACIII: 22 CNGA2: 68.9 ANO2 (Fig. 8*B*). Almost identical results were obtained from the WT littermates, except for the undetectable amount of M71-OR in these animals (Fig. 8 *A*, *Right* and Fig. 8*B*).

As a calibration, we also examined side by side the protein amounts of the tetrameric CNG channel's three constituent subunits. We obtained a molecular total of $(0.42 \pm 0.14) \times 10^{12}$ CNGA2, $(0.22 \pm 0.05) \times 10^{12}$ CNGA4, and $(0.17 \pm 0.05) \times 10^{12}$ CNGB1 in M71-monoclonal-nose ORN cilia, with almost identical numbers found in WT ORNs (*SI Appendix*, Fig. S9). This channel stoichiometry is consistent with two CNGA2: one CNGA4: one CNGB1 reported by others (62).

Finally, each native Ca^{2+}-activated Cl channel is known to comprise two ANO2 subunits (63). Hence, taken altogether, we can rewrite the protein mole ratios as 100 M71-OR: 1,422 G_{olf}: 54.5 ACIII: 11 CNG channels: 34.5 Ca^{2+}-activated Cl channels. Based on our estimated density of M71-OR being ~1,000 μm^{-2}, we obtain 110 CNG channels per square micrometer and 345 Ca^{2+}-activated Cl channels per square micrometer.

Thus, overall, in units of molecules per square micrometer on cilia membrane, we have 1,000 M71-OR: 14,220 G_{olf}: 545 ACIII: 110 CNG channels: 345 Ca^{2+}-activated Cl channels (Fig. 8*C*).

Discussion

Low Signaling Probability at Odorant/OR*-to-$G\alpha_{olf}$*/ACIII* Effector Step. The near-uniform presence of M71-expressing ORNs in the main olfactory epithelium of the M71-monoclonal-nose mouse provides a unique opportunity for measuring biochemically the so-far unknown number of OR molecules in an ORN by using M71-OR as a proxy. With this mouse, we have arrived at $\sim 2 \times 10^5$ M71-OR molecules on the cilia of an intact ORN, with a density of ~1,000 molecules per square micrometer. It would be interesting to know in the future whether this M71-OR density is representative of various OR species in the mouse main olfactory epithelium, or whether differences exist depending on the specific function of a given OR.

Applying the above total number of M71-OR molecules per ORN to our experimental data and adopting a nominal consequential (i.e., leading to complex formation) aqueous bimolecular collision rate of 10^8 $M^{-1} \cdot s^{-1}$, we estimated that only one in $\sim 10^4$ acetophenone/M71-OR complexes would successfully lead to an elementary electrical response, triggered by one $G\alpha_{olf}$*/ACIII* effector complex (see *Results* for details). More conservatively, by borrowing a wider range of known k_{on} rates in enzyme–substrate reactions, we arrived at a success probability of 10^{-2} to 10^{-5}, still very low even at the upper end (*Results*). In any case, regardless of the assumptions in the above calculations, the simple conclusion of a low probability $\ll 1$ generally holds based on the experiments of Fig. 4, unless extremely efficient odorants for M71-OR remain at large after much prior searching effort (34, 35).

At this point, we speculate that the low probability of successful transduction (i.e., the weak link) likely originates, parsimoniously, from 1) an extremely low percentage of odorant/receptor collisions that are consequential, 2) a low dwell time of odorant on M71-OR (hence odorant/M71-OR effector complex lifetime), and/or 3) a low efficiency of the odorant/M71-OR complex in activating G_{olf} upon encounter. On the other hand, the signal transmission from $G\alpha_{olf}$* to the $G\alpha_{olf}$*/ACIII* effector is likely highly efficient,

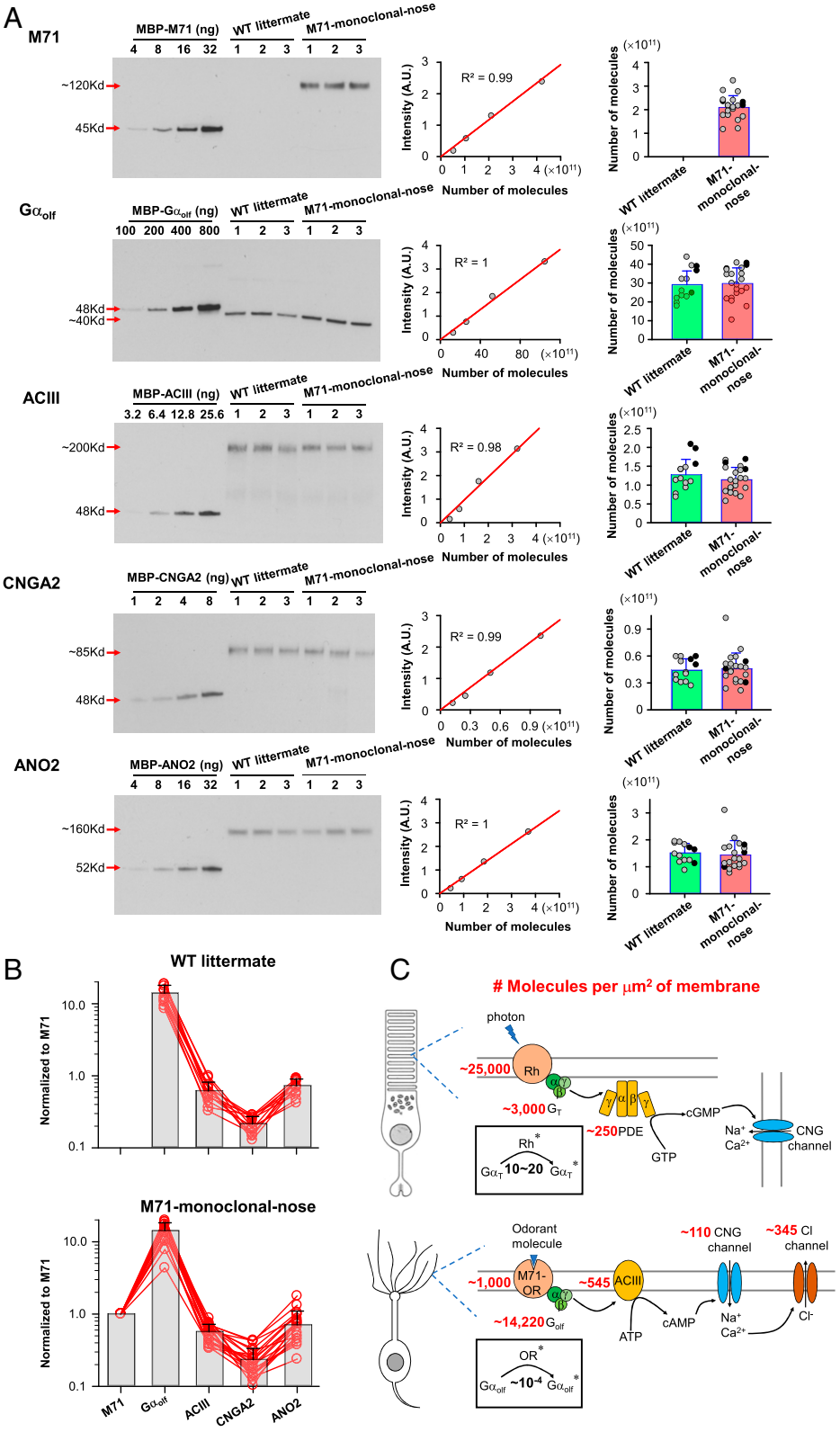

Fig. 8. Quantification of absolute protein amounts of downstream key olfactory-transduction components in WT littermate and M71-monoclonal ORNs. (*A*, *Left*) Representative Western blot images showing successive dilutions of standard proteins (MBP-M71 [45 kD], MBP-$G\alpha_{olf}$ [48 kD], MBP-ACIII [48 kD], MBP-CNGA2 [48 kD], and MBP-ANO2 [48 kD]), as well as 1/10th of ciliary proteins from three individual M71-monoclonal mice and three littermate WT mice in the same blots. (*A*, *Middle*) The signal intensities of different amounts of MBP standard proteins plotted against the number of molecules (gray dots). The standard curves (red) are straight lines. (*A*, *Right*) Collective data of the number of molecules of M71, $G\alpha_{olf}$, ACIII, CNGA2, and ANO2 in 1/10th ciliary proteins from M71-monoclonal (n = 21) and littermate WT (n = 13) mice. Bars indicate mean ± SD. Black dots are the values from the experiment on the *Left*. M71 protein was below detection in WT mice. (*B*) Mole ratios of M71, $G\alpha_{olf}$, ACIII, CNGA2, and ANO2 in WT (*Upper*) and M71-monoclonal (*Lower*) mice, all normalized against the M71-OR level in M71-monoclonal-nose mice. Bars indicate mean ± SD. Circles indicate individual mice. Each line connects data from the same mouse. (*C*) Schematics showing the protein mole ratios in rod phototransduction and olfactory transduction. See main text.

by analogy to rod phototransduction, where the measured number of $G\alpha_{T1}$*/cGMP-PDE* effectors generated per rhodopsin [~10 to 20 (3, 4)] appears to be similar to the (temperature-corrected) estimated number of $G\alpha_{T1}$*s produced (64).

Generalization to Other Ligand-Triggered GPCR Signaling: Rod Phototransduction May Be Unique. Whether the low signaling probability that we found for M71-OR applies to other ORs in olfactory transduction or to other ligand-triggered GPCR pathways is unknown at present. In the majority of cases, the native endogenous ligand (such as a hormone or neurotransmitter) for a given GPCR inside the body is already in place, unlike the broad range of native and nonnative odorants potentially encountered by an OR under our experimental conditions. Ultimately, this question for any particular GPCR pathway can only be answered by detailed experimental analysis as what we

have done. On the other hand, it seems reasonable to suppose that, in most GPCR-signaling situations, not every complex between a ligand molecule and its GPCR has to be effective. Presumably, the typical physiological signal may simply be the collective output from a population of a given GPCR species in question, whether located over the entire cell [such as β_1-adrenergic receptors on a cardiac myocyte (65)] or on a selective part of the cell (such as a cluster of metabotropic receptors at a synapse). As such, a cellular function may already be well-served when a fraction—even just a small fraction—of the GPCR ensemble sends an output signal successfully, no different from the collective signal from an ion-channel population. In the scenario considered here, a collective macroscopic signal originating from all M71-OR molecules on an ORN will potentially increase the single M71-OR's molecular output by 2×10^5 times. Additionally, the axonal convergence of on average $\sim 10^4$ ORNs expressing the same OR species (i.e., $\sim 10^7$ ORNs divided by $\sim 10^3$ OR species) to the same synaptic glomerulus or pair of glomeruli in the olfactory bulb will provide a further boost to the signal.

By contrast, rods mediating dim-light vision require not only exquisite sensitivity down to the single-photon detection level but also sufficient spatial acuity for seeing images. This dual requirement necessitates single-rhodopsin signaling but also limited signal convergence, possibly explaining a built-in, high amplification within a given rod at the G protein step (see also next section). In this regard, a comparison between rod vision and cone vision is helpful. Cones mediate vision in higher light conditions, and thus do not need the ability to signal a single photon. Correspondingly, one photoexcited cone pigment molecule may activate on average less than one cone $G\alpha_{T2}$ (cone transducin)*/cGMP-PDE* effector complex (66). As such, cone phototransduction is more in line with olfactory transduction than with rod phototransduction.

If necessary, there are also ways to enhance GPCR signaling at the macroscopic level. For example, the density of a GPCR on the surface membrane can be scaled up. Compared with rhodopsin, which has a density of $\sim 25{,}000\ \mu m^{-2}$ on the light-sensitive retinal rod outer-segment membrane (67), the M71-OR density on the ORN's ciliary surface is only $\sim 1{,}000\ \mu m^{-2}$, with potential room for a much higher density. It would be interesting to see whether this alternative strategy is indeed used by some ORNs requiring exceptionally high sensitivity, such as to a pheromone. The total number of ORNs expressing a given OR also does not appear to be constant, thus providing further flexibility when necessary (48).

Mole Ratios of Proteins in Olfactory-Transduction Signaling. In this work, we have measured the mole ratios of the olfactory-transduction proteins to be ~100 M71-OR: 1,422 G_{olf}: 54.5 ACIII: 11 CNG channels: 34.5 Ca^{2+}-activated Cl channels. Converting into molecules per square micrometer of ciliary surface membrane, we have roughly 1,000 M71-OR: 14,220 G_{olf}: 545 ACIII: 110 CNG channels: 345 Ca^{2+}-activated Cl channels. These numbers are derived based on the assumption of a uniform density of these proteins along the cilia, which is supported by our finding shown in Fig. 6*E*. The densities we found for the CNG channel and the Ca^{2+}-activated Cl channel are quite different from previous estimates from amphibians and rat (68–70), but probably more reliable because our measurements were quite straightforward.

Apart from being useful for mathematical modeling of olfactory transduction as a representative in-depth analysis of ligand-triggered GPCR signaling [as has been carried out extensively for rod phototransduction (67, 71–73)], our protein quantifications are informative for contrasting with mammalian rod phototransduction. For the latter, in units of molecules per square micrometer of outer-segment disk membrane, the values are roughly 25,000 rhodopsins: 3,000 G_{T1}: 250 cGMP PDE (dimer): ~170 CNG channels [see ref. 67 for a review; the value for CNG channels was obtained from amphibian rods (74)]. The much higher rhodopsin density is not surprising given its small molecular cross-section for photon capture and its strict one-time encounter with photons, be it success or failure. The pronounced ~5-fold higher G_{olf} than G_{T1} protein density on the membrane, on the other hand, is interesting. The implication is that, at low stimulus strengths, an activated odorant/OR* complex should have a much higher probability than does rhodopsin* in encountering its corresponding G protein, assuming similar membrane fluidity and other parameters. Our interpretation here is that nature may have already taken the task of increasing the success probability at the G protein–activation step in olfactory transduction, albeit still giving a low probability overall because of other factors (see first section in *Discussion*). In adult rat ventricular myocytes, where prototypical GPCR signaling occurs, the mole ratio of β_1-adrenergic receptor:$G\alpha_s$:adenylyl cyclase was reported to be 1:224:3 (75), with an even higher amount of G_s, although the overall signaling efficiency in this pathway remains unknown.

Materials and Methods

Animals, solutions, recordings, immunohistochemistry, Western blotting, and other experimental details are provided in *SI Appendix, Materials and Methods*.

Data Availability. All study data are included in the article and/or *SI Appendix*.

ACKNOWLEDGMENTS. We thank T.B. for kindly providing the *M71-IRES-tauGFP* mouse line, Dr. Gilad Barnea for an antibody against M71-OR, Dr. Martin Biel for those against CNGA4 and CNGB1b, Dr. James Cherry for that against PDE4A, and Dr. Joseph Beavo for that against PDE1C. Dr. Xiaojun Li kindly tested the antibody that we subsequently generated commercially against M71-OR, based on Dr. Barnea's. T.B. and Hiroaki Matsunami kindly suggested to us certain potentially very effective odorants for M71-OR. We are also grateful to E.R. for helpful discussions on GPCR signaling in general; Drs. Brian Camley, Howard C. Berg, and Markus Meister for illuminating discussions on diffusion-limited collisions; Michael Delannoy of the Johns Hopkins Microscope Facility for providing guidance for the electron microscopy experiments; and Dr. Michele Pucak of the Multiphoton Imaging Core at Johns Hopkins (NIH Grant P30 NS050274) for imaging and data analysis. We thank Dr. Yair Ben-Chaim for early preliminary experiments on the M71-monoclonal-nose mouse line, Terry Shelley for fabricating all custom equipment, and Liusong Ding for mouse genotyping. Finally, we thank Drs. Fred Rieke, Michael Tri Do, Dong-Gen Luo, Tsung-Yu Chen, Zheng Jiang, Haiqing Zhao, and Randy Reed for helpful suggestions and discussions, as well as Drs. Zuying Chai, Guang Li, Daniel Silverman, Wendy Yue, Lujing Chen, Yanghui Sheng, and Yaqing Ye of the K.-W.Y. laboratory for comments on the manuscript. This work was supported by NIH Grant R01 DC14941 (to K.-W.Y.) and Canadian Institutes of Health Research Grant PJT 148649 (to R.S.M.). We are grateful to the two reviewers for their detailed and helpful comments.

Author affiliations: [a]Solomon H. Snyder Department of Neuroscience, Johns Hopkins University School of Medicine, Baltimore, MD 21205; [b]Department of Biochemistry and Molecular Biology, University of British Columbia, Vancouver, BC V6T 1Z3, Canada; [c]Neuroscience Graduate Program, Johns Hopkins University School of Medicine, Baltimore, MD 21205; and [d]Department of Neuroscience, Brown University, Providence, RI 02912

1. T. M. Vuong, M. Chabre, L. Stryer, Millisecond activation of transducin in the cyclic nucleotide cascade of vision. *Nature* **311**, 659–661 (1984).
2. D. A. Baylor, T. D. Lamb, K.-W. Yau, Responses of retinal rods to single photons. *J. Physiol.* **288**, 613–634 (1979).
3. W. W. S. Yue *et al.*, Elementary response triggered by transducin in retinal rods. *Proc. Natl. Acad. Sci. U.S.A.* **116**, 5144–5153 (2019).
4. V. Y. Arshavsky, M. E. Burns, Current understanding of signal amplification in phototransduction. *Cell. Logist.* **4**, e29390 (2014).
5. V. Bhandawat, J. Reisert, K.-W. Yau, Elementary response of olfactory receptor neurons to odorants. *Science* **308**, 1931–1934 (2005).
6. S. J. Kleene, The electrochemical basis of odor transduction in vertebrate olfactory cilia. *Chem. Senses* **33**, 839–859 (2008).
7. S. D. Munger, T. Leinders-Zufall, F. Zufall, Subsystem organization of the mammalian sense of smell. *Annu. Rev. Physiol.* **71**, 115–140 (2009).
8. J. Reisert, H. Zhao, Perspectives on: Information and coding in mammalian sensory physiology: Response kinetics of olfactory receptor neurons and the implications in olfactory coding. *J. Gen. Physiol.* **138**, 303–310 (2011).
9. L. Buck, R. Axel, A novel multigene family may encode odorant receptors: A molecular basis for odor recognition. *Cell* **65**, 175–187 (1991).
10. D. T. Jones, R. R. Reed, G_{olf}: An olfactory neuron specific-G protein involved in odorant signal transduction. *Science* **244**, 790–795 (1989).
11. H. A. Bakalyar, R. R. Reed, Identification of a specialized adenylyl cyclase that may mediate odorant detection. *Science* **250**, 1403–1406 (1990).
12. T. Nakamura, G. H. Gold, A cyclic nucleotide-gated conductance in olfactory receptor cilia. *Nature* **325**, 442–444 (1987).
13. R. S. Dhallan, K.-W. Yau, K. A. Schrader, R. R. Reed, Primary structure and functional expression of a cyclic nucleotide-activated channel from olfactory neurons. *Nature* **347**, 184–187 (1990).
14. S. J. Kleene, R. C. Gesteland, Calcium-activated chloride conductance in frog olfactory cilia. *J. Neurosci.* **11**, 3624–3629 (1991).
15. A. B. Stephan *et al.*, ANO2 is the cilial calcium-activated chloride channel that may mediate olfactory amplification. *Proc. Natl. Acad. Sci. U.S.A.* **106**, 11776–11781 (2009).
16. S. Rasche *et al.*, Tmem16b is specifically expressed in the cilia of olfactory sensory neurons. *Chem. Senses* **35**, 239–245 (2010).
17. K. Dauner, J. Lissmann, S. Jeridi, S. Frings, F. Möhrlen, Expression patterns of anoctamin 1 and anoctamin 2 chloride channels in the mammalian nose. *Cell Tissue Res.* **347**, 327–341 (2012).
18. T. Kurahashi, K.-W. Yau, Co-existence of cationic and chloride components in odorant-induced current of vertebrate olfactory receptor cells. *Nature* **363**, 71–74 (1993).
19. A. B. Zhainazarov, B. W. Ache, Odor-induced currents in *Xenopus* olfactory receptor cells measured with perforated-patch recording. *J. Neurophysiol.* **74**, 479–483 (1995).
20. R. C. Li, Y. Ben-Chaim, K.-W. Yau, C. C. Lin, Cyclic-nucleotide-gated cation current and Ca^{2+}-activated Cl current elicited by odorant in vertebrate olfactory receptor neurons. *Proc. Natl. Acad. Sci. U.S.A.* **113**, 11078–11087 (2016).
21. R. C. Li *et al.*, Ca^{2+}-activated Cl current predominates in threshold response of mouse olfactory receptor neurons. *Proc. Natl. Acad. Sci. U.S.A.* **115**, 5570–5575 (2018).
22. H. Kaneko, I. Putzier, S. Frings, U. B. Kaupp, T. Gensch, Chloride accumulation in mammalian olfactory sensory neurons. *J. Neurosci.* **24**, 7931–7938 (2004).
23. J. Reisert, J. Lai, K. W. Yau, J. Bradley, Mechanism of the excitatory Cl^- response in mouse olfactory receptor neurons. *Neuron* **45**, 553–561 (2005).
24. T. Hengl *et al.*, Molecular components of signal amplification in olfactory sensory cilia. *Proc. Natl. Acad. Sci. U.S.A.* **107**, 6052–6057 (2010).
25. C. Jaén, M. H. Ozdener, J. Reisert, Mechanisms of chloride uptake in frog olfactory receptor neurons. *J. Comp. Physiol. A Neuroethol. Sens. Neural Behav. Physiol.* **197**, 339–349 (2011).
26. C. Yan *et al.*, Molecular cloning and characterization of a calmodulin-dependent phosphodiesterase enriched in olfactory sensory neurons. *Proc. Natl. Acad. Sci. U.S.A.* **92**, 9677–9681 (1995).
27. J. A. Cherry, R. L. Davis, A mouse homolog of dunce, a gene important for learning and memory in *Drosophila*, is preferentially expressed in olfactory receptor neurons. *J. Neurobiol.* **28**, 102–113 (1995).
28. J. Reisert, H. R. Matthews, Na^+-dependent Ca^{2+} extrusion governs response recovery in frog olfactory receptor cells. *J. Gen. Physiol.* **112**, 529–535 (1998).
29. S. Antolin, H. R. Matthews, The effect of external sodium concentration on sodium-calcium exchange in frog olfactory receptor cells. *J. Physiol.* **581**, 495–503 (2007).
30. S. J. Kleene, Limits of calcium clearance by plasma membrane calcium ATPase in olfactory cilia. *PLoS One* **4**, e5266 (2009).
31. S. Antolin, J. Reisert, H. R. Matthews, Olfactory response termination involves Ca^{2+}-ATPase in vertebrate olfactory receptor neuron cilia. *J. Gen. Physiol.* **135**, 367–378 (2010).
32. A. B. Stephan *et al.*, The Na^+/Ca^{2+} exchanger NCKX4 governs termination and adaptation of the mammalian olfactory response. *Nat. Neurosci.* **15**, 131–137 (2011).
33. A. Fleischmann *et al.*, Mice with a "monoclonal nose": Perturbations in an olfactory map impair odor discrimination. *Neuron* **60**, 1068–1081 (2008).
34. T. Bozza, P. Feinstein, C. Zheng, P. Mombaerts, Odorant receptor expression defines functional units in the mouse olfactory system. *J. Neurosci.* **22**, 3033–3043 (2002).
35. J. Zhang, G. Huang, A. Dewan, P. Feinstein, T. Bozza, Uncoupling stimulus specificity and glomerular position in the mouse olfactory system. *Mol. Cell. Neurosci.* **51**, 79–88 (2012).
36. J. Bubnell *et al.*, In vitro mutational and bioinformatics analysis of the M71 odorant receptor and its superfamily. *PLoS One* **10**, e0141712 (2015).
37. X. Zhang, S. Firestein, The olfactory receptor gene superfamily of the mouse. *Nat. Neurosci.* **5**, 124–133 (2002).
38. P. A. Godfrey, B. Malnic, L. B. Buck, The mouse olfactory receptor gene family. *Proc. Natl. Acad. Sci. U.S.A.* **101**, 2156–2161 (2004).
39. F. L. Margolis, A brain protein unique to the olfactory bulb. *Proc. Natl. Acad. Sci. U.S.A.* **69**, 1221–1224 (1972).
40. K. Kuhlmann *et al.*, The membrane proteome of sensory cilia to the depth of olfactory receptors. *Mol. Cell. Proteomics* **13**, 1828–1843 (2014).
41. B. W. Lipscomb, H. B. Treloar, C. A. Greer, Cell surface carbohydrates reveal heterogeneity in olfactory receptor cell axons in the mouse. *Cell Tissue Res.* **308**, 7–17 (2002).
42. S. Lomvardas *et al.*, Interchromosomal interactions and olfactory receptor choice. *Cell* **126**, 403–413 (2006).
43. V. Bhandawat, J. Reisert, K. W. Yau, Signaling by olfactory receptor neurons near threshold. *Proc. Natl. Acad. Sci. U.S.A.* **107**, 18682–18687 (2010).
44. Y. Ben-Chaim, M. M. Cheng, K. W. Yau, Unitary response of mouse olfactory receptor neurons. *Proc. Natl. Acad. Sci. U.S.A.* **108**, 822–827 (2011).
45. R. S. Molday, L. L. Molday, Identification and characterization of multiple forms of rhodopsin and minor proteins in frog and bovine rod outer segment disc membranes. Electrophoresis, lectin labeling, and proteolysis studies. *J. Biol. Chem.* **254**, 4653–4660 (1979).
46. S. Firestein, How the olfactory system makes sense of scents. *Nature* **413**, 211–218 (2001).
47. K. Kawagishi *et al.*, Stereological quantification of olfactory receptor neurons in mice. *Neuroscience* **272**, 29–33 (2014).
48. O. C. Bressel, M. Khan, P. Mombaerts, Linear correlation between the number of olfactory sensory neurons expressing a given mouse odorant receptor gene and the total volume of the corresponding glomeruli in the olfactory bulb. *J. Comp. Neurol.* **524**, 199–209 (2016).
49. T. Kaneko-Goto *et al.*, Goofy coordinates the acuity of olfactory signaling. *J. Neurosci.* **33**, 12987–12996 (2013).
50. K. Ukhanov *et al.*, INPP5E controls ciliary localization of phospholipids and the odor response in olfactory sensory neurons. *J. Cell Sci.* **135**, jcs258364 (2022).
51. H. Gutfreund, *Kinetics for the Life Sciences* (Cambridge University Press, Cambridge, UK, 1995).
52. H. Takeuchi, T. Kurahashi, Second messenger molecules have a limited spread in olfactory cilia. *J. Gen. Physiol.* **150**, 1647–1659 (2018).
53. H. C. Berg, E. M. Purcell, Physics of chemoreception. *Biophys. J.* **20**, 193–219 (1977).
54. H. C. Berg, *Random Walks in Biology* (Princeton University Press, Princeton, NJ, expanded ed., 1993).
55. A. Fersht, *Enzyme Structure and Mechanism* (W. H. Freeman and Company, ed. 2, 1985).
56. C. M. Krispel *et al.*, RGS expression rate-limits recovery of rod photoresponses. *Neuron* **51**, 409–416 (2006).
57. A. Kato, J. Reisert, S. Ihara, K. Yoshikawa, K. Touhara, Evaluation of the role of G protein-coupled receptor kinase 3 in desensitization of mouse odorant receptors in a mammalian cell line and in olfactory sensory neurons. *Chem. Senses* **39**, 771–780 (2014).
58. J. T. Finn, M. E. Grunwald, K.-W. Yau, Cyclic nucleotide-gated ion channels: An extended family with diverse functions. *Annu. Rev. Physiol.* **58**, 395–426 (1996).
59. I. Masuho *et al.*, A global map of G protein signaling regulation by RGS proteins. *Cell* **183**, 503–521.e19 (2020).
60. D. R. Brandt, E. M. Ross, Catecholamine-stimulated GTPase cycle. Multiple sites of regulation by beta-adrenergic receptor and Mg^{2+} studied in reconstituted receptor-Gs vesicles. *J. Biol. Chem.* **261**, 1656–1664 (1986).
61. A. J. Kimple, D. E. Bosch, P. M. Giguère, D. P. Siderovski, Regulators of G-protein signaling and their Gα substrates: Promises and challenges in their use as drug discovery targets. *Pharmacol. Rev.* **63**, 728–749 (2011).
62. J. Zheng, W. N. Zagotta, Stoichiometry and assembly of olfactory cyclic nucleotide-gated channels. *Neuron* **42**, 411–421 (2004).
63. J. Tien, H. Y. Lee, D. L. Minor Jr., Y. N. Jan, L. Y. Jan, Identification of a dimerization domain in the TMEM16A calcium-activated chloride channel (CaCC). *Proc. Natl. Acad. Sci. U.S.A.* **110**, 6352–6357 (2013).
64. I. B. Leskov *et al.*, The gain of rod phototransduction: Reconciliation of biochemical and electrophysiological measurements. *Neuron* **27**, 525–537 (2000).
65. R. P. Xiao *et al.*, Subtype-specific alpha1- and beta-adrenoceptor signaling in the heart. *Trends Pharmacol. Sci.* **27**, 330–337 (2006).
66. D. G. Luo *et al.*, Apo-opsin and its dark constitutive activity across retinal cone subtypes. *Curr. Biol.* **30**, 4921–4931.e5 (2020).
67. E. N. Pugh Jr., T. D. Lamb, Amplification and kinetics of the activation steps in phototransduction. *Biochim. Biophys. Acta* **1141**, 111–149 (1993).
68. T. Kurahashi, A. Kaneko, High density cAMP-gated channels at the ciliary membrane in the olfactory receptor cell. *Neuroreport* **2**, 5–8 (1991).
69. H. P. Larsson, S. J. Kleene, H. Lecar, Noise analysis of ion channels in non-space-clamped cables: Estimates of channel parameters in olfactory cilia. *Biophys. J.* **72**, 1193–1203 (1997).
70. J. Reisert, P. J. Bauer, K. W. Yau, S. Frings, The Ca-activated Cl channel and its control in rat olfactory receptor neurons. *J. Gen. Physiol.* **122**, 349–363 (2003).
71. R. D. Hamer, S. C. Nicholas, D. Tranchina, T. D. Lamb, J. L. Jarvinen, Toward a unified model of vertebrate rod phototransduction. *Vis. Neurosci.* **22**, 417–436 (2005).
72. J. Reingruber *et al.*, Detection of single photons by toad and mouse rods. *Proc. Natl. Acad. Sci. U.S.A.* **110**, 19378–19383 (2013).
73. J. Reingruber, N. T. Ingram, K. G. Griffis, G. L. Fain, A kinetic analysis of mouse rod and cone photoreceptor responses. *J. Physiol.* **598**, 3747–3763 (2020).
74. J. W. Karpen, D. A. Loney, D. A. Baylor, Cyclic GMP-activated channels of salamander retinal rods: Spatial distribution and variation of responsiveness. *J. Physiol.* **448**, 257–274 (1992).
75. S. R. Post, R. Hilal-Dandan, K. Urasawa, L. L. Brunton, P. A. Insel, Quantification of signalling components and amplification in the beta-adrenergic-receptor-adenylate cyclase pathway in isolated adult rat ventricular myocytes. *Biochem. J.* **311**, 75–80 (1995).